The 8th International Conference on Jets, Wakes and Separated Flows, ICJWSF-2024
September 23-25, 2024, Firenze, Italy

Large Eddy Simulation of Underexpanded Microjets from a Square Supersonic Nozzle

R. Nishi[1*], I. Morita[1], Y. Kimura[2], S. Nakao[1], Y. Miyazato[1], and Y. Ishino[3]

1: Dept. of Mechanical Systems Engineering, The University of Kitakyushu, Japan
2: Dept. of Mechanical Systems Engineering,
The University of Kitakyushu (Currently AIST Solution), Japan
3: Dept. of Mechanical Engineering, Nagoya Institute of Technology, Japan

* Corresponding author: ryuki-ichigo@i.softbank.jp

Abstract

Underexpanded microjet issuing from a square Laval nozzle of a design Mach number of 1.5 is quantitatively visualized by rainbow schlieren tomography. The test nozzle has a channel area of 1 mm$\times$1 mm at the exit, and an equivalent diameter of 1.13 mm. Flow visualization is performed at a nozzle pressure ratio of 7.0 to produce strong shocks in the jet plume. The Reynolds number based upon the equivalent diameter and flow properties at the nozzle exit is 9.37×10^5. Multi-view rainbow schlieren pictures with the horizontal filter setting are taken by rotating the nozzle around its central axis at an equal interval of 5° ranging from 0 to 180°. The jet density field is reconstructed by the convolution back projection method. The flow features of shock-containing square jets are demonstrated.

Keywords:*Large eddy simulation, Square Laval nozzle, Shock wave, Microjet.*

1. Introduction

In recent years, there has been considerable research on the subject of the dynamics of a supersonic microjet for the application of microscale devices, including a critical nozzle for obtaining mass-flow rate at a low Reynolds number, a micropump based on the principle of macroscopic vapor-jet and diffusion-pump, a small satellite thruster in space engineering, gas wiping nozzles for continuous galvanizing line, etc. A deep, detailed comprehension of the flow characteristics through such devices requires information regarding the quantitative velocity, density, and temperature measurements in the flow field. However, even for supersonic jets from macroscale round nozzles, the jet characteristics are almost only qualitatively known [1].

Nazari et al. [2] experimentally investigated instantaneous three-dimensional structures of microjets issuing from round and square Laval nozzles operating under design and off-design conditions. They quantitatively measured the three-dimensional density fields of the microjets using 20 schlieren optical systems placed at equal intervals around the nozzle. To the best of the authors' knowledge, there are no studies on the unsteady three-dimensional structure of microjets emerging from square nozzles. It is very difficult to experimentally clarify unsteady flow features of a microjet issuing from an asymmetric nozzle. Therefore, in this study, large eddy simulation (LES) is performed to understand the unsteady flow structures of shock-containing square microjets.

2. Experimental Methods

Experiments are conducted in an intermittent blowdown compressed-air facility. Ambient air is pressurized by a compressor up to 1 MPa and stored in a high-pressure reservoir comprising two storage tanks with a total capacity of 2 m^3 after filtering and drying. The high-pressure dry air enters a plenum chamber through the coupling shown in Fig. 1, reaches a stagnation state. It is then discharged into the quiescent air after accelerated to supersonic speed through a test nozzle that can be rotated about its central axis [3].

As shown in Fig. 2, a Laval nozzle with a square cross-section of 1 mm height by 1 mm width at the exit and a design Mach number of 1.5 is used as a test nozzle. The upper and lower wall contours from the nozzle

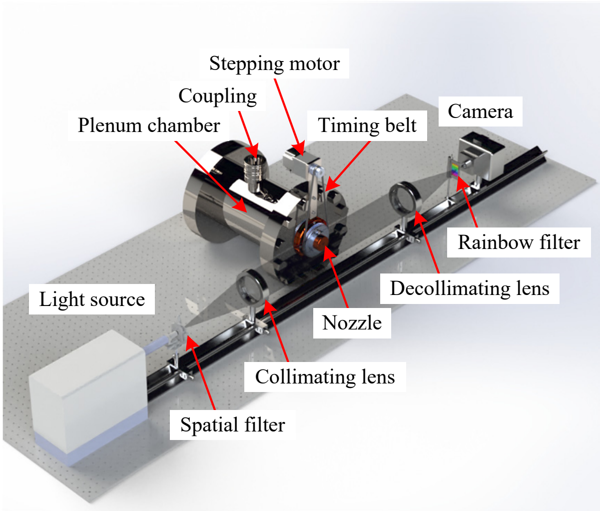

Fig. 1: Schematic diagram of the experimental apparatus with rainbow schlieren optical system

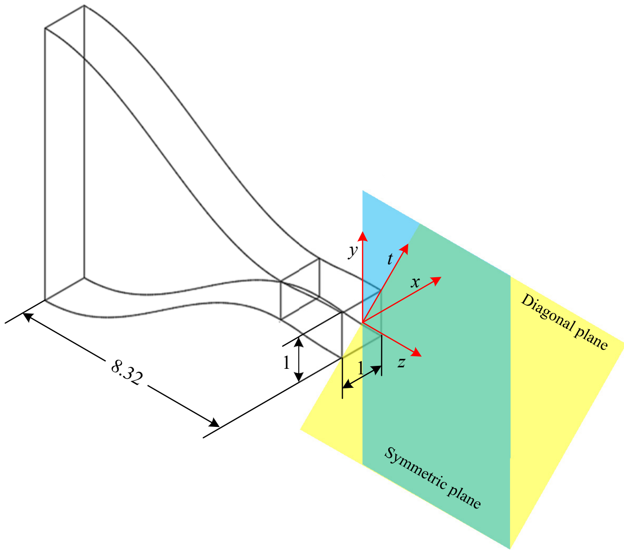

Fig. 2: Schematic diagram of a test nozzle with a coordinate system.

inlet to the throat are designed by a sinusoidal curve to provide uniform flows at the nozzle inlet and throat. In addition, the upper and lower wall contours from the throat to exit are designed based on the method of characteristics to provide smooth uniform flows at the exit. The spanwise width of the nozzle is held constant at 1 mm over a full length of 8.32 mm in the flow direction. The equivalent diameter at the nozzle exit, which is given by $D_{eq} = (4/\pi)^{1/2}$ for the present nozzle, is approximately 1.13 mm where the D_{eq} is defined as the diameter of a virtual circular nozzle with a cross-sectional area equal to that of the actual nozzle [4]. As shown in Fig. 2, a Cartesian coordinate system (x, y, z) is used, with the origin 'O' at the center in the cross-section of the nozzle exit, the 'x' axis in the horizontal direction, the 'y' axis in the vertical direction (perpendicular to the x axis), and the 'z' axis in the flow direction. In addition, we refer to the yz-plane including the z-axis as the symmetric plane and the plane inclined 45 degrees from the symmetric plane as the diagonal plane. As shown in Fig. 2, the t-axis is taken perpendicular to the z-axis along the diagonal plane. Furthermore, we refer to the observation of a flow field perpendicular to the symmetry plane as the symmetry plane view and that perpendicular to the diagonal plane as the diagonal plane view.

The nozzle pressure ratio (NPR), which is defined as the ratio of the stagnation pressure (p_{os}) upstream of the nozzle to the back pressure (p_b) is achieved by changing the p_{os}, with the p_b held constant at NPR = 4.0 to produce an underexpanded jet with a fully expanded Mach number of M_j = 1.93. For the present nozzle, the theoretical nozzle pressure ratio to realize the shock free jet or the design nozzle pressure ratio is

approximately 3.67 for γ = 1.4. In the present experiments, p_b is 101.3 kPa and the ambient temperature T_b is 300 K. The Reynolds number, based upon the equivalent diameter and flow properties at the nozzle exit, is 6.76×10^4. Quantitative flow visualization is performed by rainbow schlieren tomography (RST) [3].
/

3. Numerical Methods

Numerical simulations are performed using the commercial computational fluid dynamics (CFD) software ANSYS Fluent Version 16.0. Microjets issuing from a square Laval nozzle with a design Mach number of 1.5 and a cross-section of 1 mm × 1 mm at the exit are numerically solved by large eddy simulation (LES) based on the Smagorinsky-Lilly model. The nozzle used in the simulation has the same geometry as in the experiment. The stagnation pressure and temperature far upstream of the nozzle, and back pressure and ambient temperature are set to p_{os} = 400 kPa, T_{os} = 300 K, p_b =101.3 kPa, and T_b = 300 K, respectively. The NPR is equal to 4.0 to produce an underexpanded free jet.

The dry air is assumed to be a perfect gas with a constant specific heat ratio of γ = 1.4, and the coefficient of viscosity is calculated by using Sutherland's law. The computational domain consists of a rectangular box of 20 × 20 × 70 mm in x-, y-, and z-direction, respectively. The block-structured mesh is generated by the mapped face meshing function equipped with ANSYS Fluent, and the total mesh count is approximatly 30 million elements. The grids around the nozzle exit, shock-cells, and shear layers are specialy refined to obtain high resolution where the minimum mesh size is approximately 5 μm. On the other hand, coarse grids with a resolution of 0.8 mm are used in areas far enough from the jet.The boundary conditions are the uniform input flow at the nozzle inlet boundary and the adiabatic no-slip on the nozzle wall, and the upper and downstream ends of the computational domain are taken as free boundaries. To ensure statistical convergence, the computation is run over at least 1,000 time steps. The simulation code is validated by quantitative comparison with the time-mean density field of the microjet obtained by rainbow schlieren deflectometry. For reference, the density field of the microjet from the LES is also quantitatively compared to that from Reynolds-averaged Navier-Stokes (RANS) simulation with the Menter's shear stress transport (SST) $k - \omega$ turbulence model. The computational domain and the minimum mesh size are the same as for the LES.

4. Results and Discussion

4.1. Density contour plots

The time-mean density contour plots of the square underexpanded microjet in the symmetric plane are represented in Fig. 3 for the (a) experiment, (b) LES, and (c) RANS. The flow direction is from left to right. The experimental density field is reproduced with a spatial resolution of approximately 2 μm. The density field from the LES is time averaged over the entire computation time. The density fields are normalized by the ambient density ρ_b. The contour level is illustrated as a color bar at the top of Fig. 3 over the range ρ/ρ_b 0.7 to 1.8 at intervals of 0.1. The black dashed line parallel to the abscissa indicates the centerline (x = y = 0 mm).

As shown in Fig. 3(a), the experimental density field shows that the dense regions appear almost equally spaced, indicating that the microjet consists of three shock cells. The thickness of the shear layer formed at the nozzle lip of the microjet gradually increases in the downstream direction. The experimental, LES and RANS density fields of the microjet are in close quantitative agreement for the first shock-cell, including the shape and density values of the expansion region. In particular, the spacing and shape of the isodensity lines within the expansion region are in extremely good quantitative agreement between the experimental and the two simulations. The LES result shows that the jet shear layer developed from the nozzle exit gradually thickens in the downstream direction, while that for RANS thickens rapidly in the downstream direction, showing a more pronounced viscous effect compared to the experiment. It can be seen that the LES quantitatively captures the experimental density field better than RANS.

4.2. Streamwise density profiles

The streamwise density profiles along the central axis of the microjet are represented in Fig. 4. The red, blue, and green solid lines denote the results obtained from the experiment, LES, and RANS, respectively. The leftward arrow shows the theoretical density ratio ($(\rho_e/\rho_b)_{th}$ = 1.58) at the nozzle exit, which is estimated based upon the assumption of the isentropic flow from the plenum chamber upstream of the nozzle to exit. In addition, the dashed line parallel to the abscissa indicates the fully expanded jet density (ρ_j/ρ_b = 1.49)

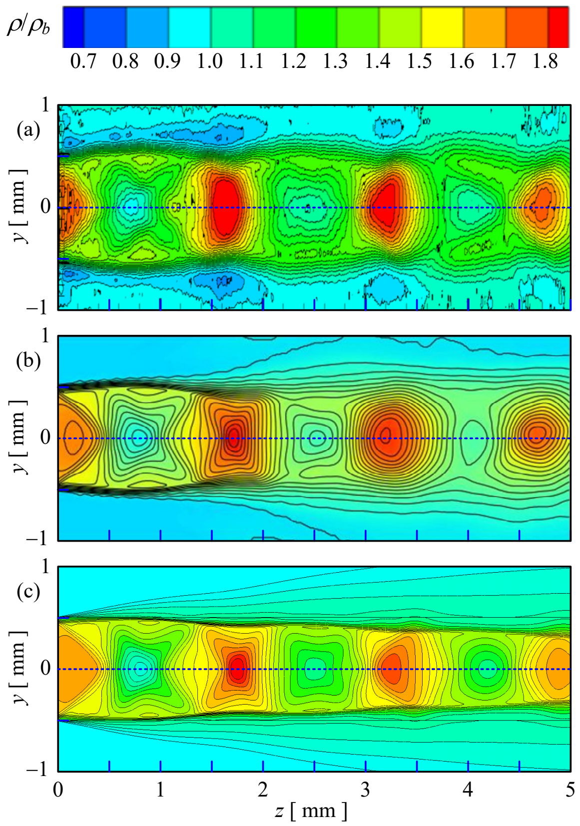

Fig. 3: Density contour plots of the square underexpanded jet in the symmetric plane at NPR = 4.0 with (a) experiment, (b) LES, and (c) RANS.

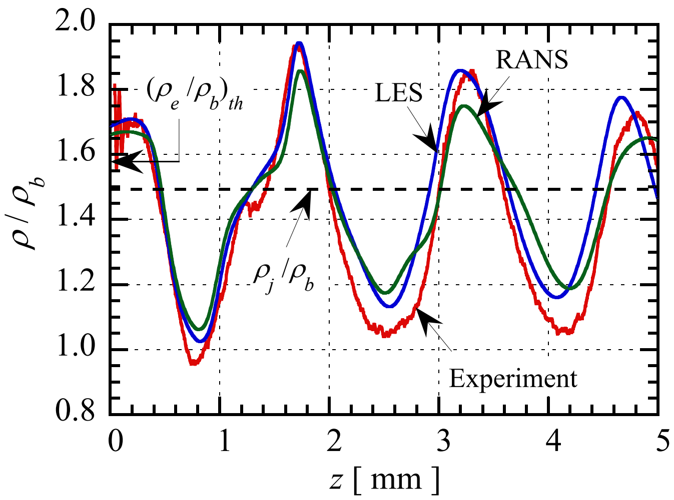

Fig. 4: Density profiles along the central axis of the square underexpanded microjet for the (a) experiment (red line), (b) LES (blue line), and RANS (green line).

normalized by the ambient density. Above the dashed line, the density is greater than the ambient density, but the static pressure is equal to the back pressure. Below this line, the static pressure is less than the back pressure.

The experimental density values near z = 0 have a large error due to the effect of light reflection at the nozzle exit plane. The experimental density along the central axis of the microjet decreases rapidly from the nozzle exit due to the expansion waves issuing from the nozzle lip and reaches a minimum value at the z = approximately 0.8 mm. The density then rises sharply due to the weak shocks in the first shock-cell and

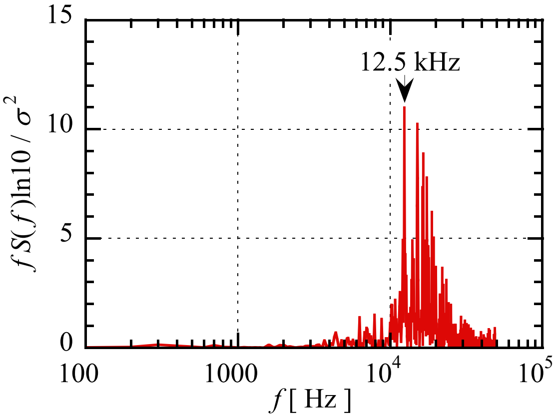

Fig. 5: Power spectral density function.

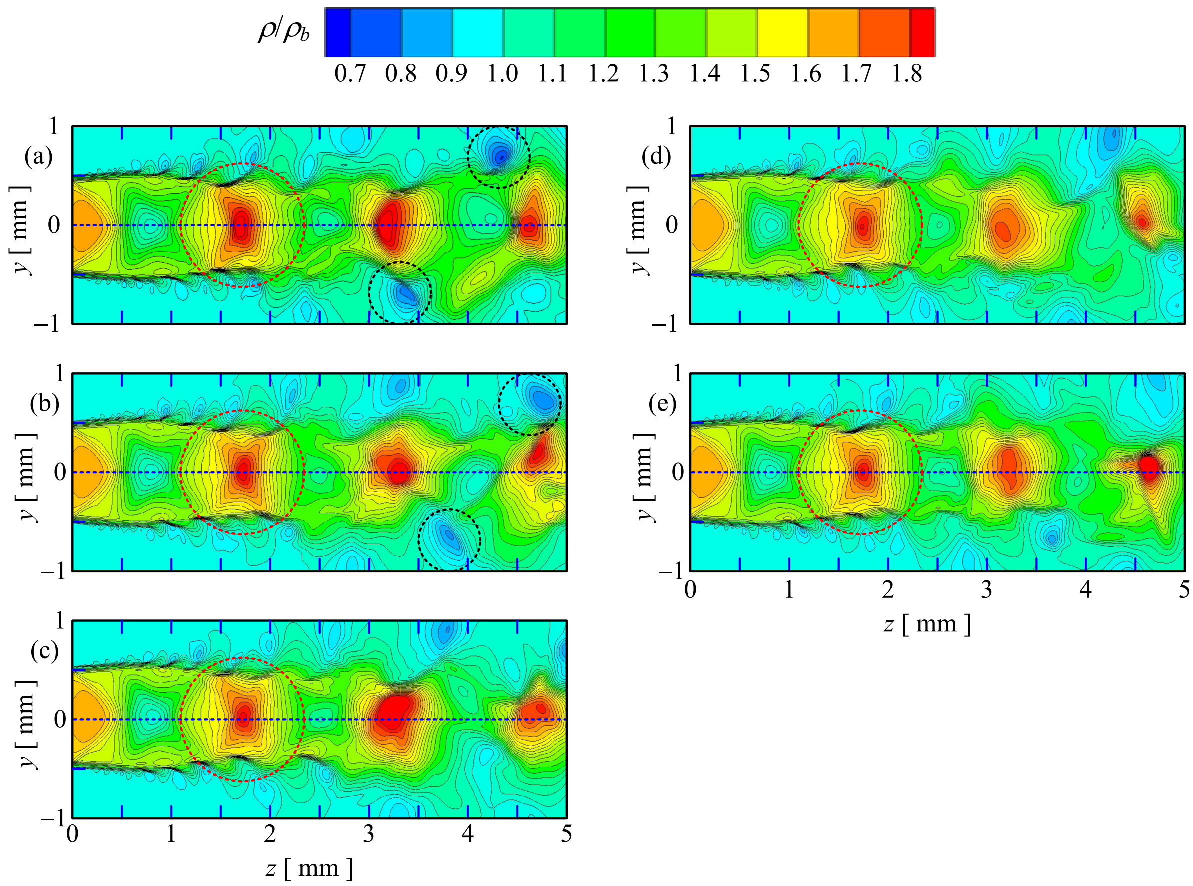

Fig. 6: Time histories of the unsteady density fields during one-oscillation cycle of the square underexpanded microjet with a dominant frequency of 12.5 kHz where (a) to (e) show the density field every 20 μs in this order.

reaches its peak value. The density variations inside the second and third shock cells are nearly the same as in the first shock-cell. The density distribution calculated by LES shows good quantitative agreement with experimental result when compared to RANS. The causes of the discrepancy between the LES and the experiment after the first shock-cell are discussed in Section 4.3.

4.3. Time histories of unsteady density fields

The oscillation spectrum of the jet was calculated from the time history of the density at $z = 4.6$ mm on the central axis of the microjet. The horizontal and vertical axes represent the frequency, $\log(f)$, and the dimensionless power spectral density function, $fS(f)\mathrm{ln}10/\sigma^2$, respectively where σ^2 indicates the variance of density fluctuation. By organizing the power spectral density function in this way, the low-frequency components become less noticeable. The high-frequency components become more prominent, and the area enclosed by the curve is 1. This can be easily confirmed from the following equation.

$$\sigma^2 = \int S(f)df = \int f \cdot S(f) \ln 10 d(\log f) \tag{1}$$

As shown in Fig. 5, the microjet oscillates with a dominant frequency of 12.5 kHz.

The time histories of the density contour plot in the symmetric plane containing the central axis of the microjet are shown for every 20 μs in Fig. 6 with the flow from left to right. This series of density fields from Figs. 6(a) to (e) corresponds to oscillations with a dominant frequency of 12.5 kHz. The shock structure circled by the red dashed line inside the first shock cell changes little with time. On the other hand, the shape of the second shock-cell is not vertically symmetric about the central axis of the jet. As can be seen from the behavior of the vortex enclosed by the black dashed line, the upper and lower jet shear layers oscillate out of phase. The unsteady flow features downstream of the first shock-cell seem to be the main reason for the quantitative disagreement between the LES and experiment for the downstream density distribution in Fig. 4.

5. Conclusions

Three-dimensional flow features of an underexpanded microjet issuing from a square Laval nozzle at a nozzle pressure ratio of 4.0 were numerically investigated by large eddy simulation (LES). The nozzle has an equivalent diameter of 1.13 mm at the exit and a design Mach number of 1.5. In addition, Reynolds-averaged Navier-Stokes simulations are performed for reference. The simulated results were validated by quantitative comparison with the time-averaged density field of the experimental data from rainbow schlieren tomography. The conclusions obtained are as follows.

(1) For the density contour in the cross-section including the central axis of the microjet, LES can quantitatively reproduce the experimental one compared to RANS. Compared to the experiment and LES, the width of the outer shear layer of the microjet simulated by RANS increases rapidly with increasing streamwise distance.

(2) The flow structure of the underexpanded microjet issuing from the nozzle exit is nearly stable in time up to the end of the compression region inside the first shock-cell, but after that location, it oscillates at a dominant frequency of 12.5 kHz.

(3) The upper and lower shear layers of the microjet downstream of the first shock-cell oscillate out of phase where periodic vortex ejections are observed from the outer shear layer of the second shock-cell.

Acknowledgments

This work was supported in part by Institute of Environmental Science and Technology, The University of Kitakyushu.

References

[1] Franquet E. et al. “Free Underexpanded Jets in a Quiescent Medium: A Review”. In: *Progress in Aerospace Sciences* 77 (2015), pp. 25–53.

[2] Nazari A. Z. et al. “Multi-Schlieren CT Measurements of Supersonic Microjets from Circular and Square Micro Nozzles”. In: *Journal of Flow Control, Measurement & Visualization* 8 (3) (2020), pp. 175–190.

[3] Fukunaga R. et al. “Application of Rainbow Schlieren Tomography for Shock-Containing Rectangular Jets”. In: *Journal of Visualization* 25 (4) (2022), pp. 687–695.

[4] Nagata T. et al. “Shock-Cell Spacings of Underexpanded Sonic Jets Emerging from Elliptic Nozzles”. In: *Experiments in Fluids* 63 (7) (2022), p. 111.